Modeling the heliospheric current sheet: Solar cycle variations

Pete Riley, J. A. Linker, and Z. Mikić

Science Applications International Corporation, San Diego, California, USA

[1]   In this report we employ an empirically driven, three-dimensional MHD model to explore the evolution of the heliospheric current sheet (HCS) during the course of the solar cycle. We compare our results with a simpler "constant-speed" approach for mapping the HCS outward into the solar wind to demonstrate that dynamic effects can substantially deform the HCS in the inner heliosphere ($\lesssim$5 AU). We find that these deformations are most pronounced at solar minimum and become less significant at solar maximum, when interaction regions are less effective. Although solar maximum is typically associated with transient, rather than corotating, processes, we show that even under such conditions, the HCS can maintain its structure over the course of several solar rotations. While the HCS may almost always be topologically equivalent to a "ballerina skirt," we discuss an interval approaching the maximum of solar cycle 23 (Carrington rotations 1960 and 1961) when the shape would be better described as "conch shell"-like. We use Ulysses magnetic field measurements to support the model results.   *INDEX TERMS:* 2162 Interplanetary Physics: Solar cycle variations (7536); 2134 Interplanetary Physics: Interplanetary magnetic fields; 2102 Interplanetary Physics: Corotating streams; 2164 Interplanetary Physics: Solar wind plasma; *KEYWORDS:* heliospheric current sheet, solar cycle variations, MHD simulations, corotating interaction regions, Ulysses, ACE, Wind

1.   Introduction

[2]   The heliospheric current sheet (HCS), a surface separating regions of opposite magnetic polarity, is a fundamental feature of the heliosphere that is intimately related to the large-scale dynamical flow of the solar wind. As the largest coherent structure within the heliosphere, the HCS is a particularly attractive entity for large-scale fluid and MHD models to follow. Although passive, it responds to the dynamics of interplanetary streams and thus provides an indirect measure of stream evolution. *Pizzo* [1994a] has pointed out that at least during relatively quiescent times and within 20 AU, corotating interaction regions (CIRs) are organized about the HCS.

[3]   The shape of the HCS also plays an important role in the modulation of galactic cosmic rays [e.g., *Jokipii*, 1997]. In addition to diffusive random walk and convection, galactic cosmic rays are subject to drift motions following the large-scale structure of the heliospheric magnetic field. In particular, during even-numbered cycles, when the northern heliospheric magnetic field is outward and the southern field is inward, positively charged particles drift inward from the polar regions and are ejected from the heliosphere along the current sheet. During odd-numbered cycles, this motion is reversed, and particles are ejected at the poles.

[4]   Previous studies investigating the large-scale morphology of the HCS have typically relied on simplified constant-speed mappings of the inferred neutral line [e.g., *Akasofu and Fry*, 1986; *Sanderson et al.*, 1999]. This approach takes some measure of the neutral line at the Sun (such as those determined from source surface models)

and maps the surface out into the heliosphere assuming that each portion of the current sheet maintains constant speed. It is thus a kinematic approach that does not take into account dynamical effects such as the acceleration of slow plasma and the deceleration of fast plasma that occurs when neighboring parcels of plasma interact. While these studies can provide a qualitative picture of the HCS, their neglect of dynamical effects could introduce significant errors. *Ho et al.* [1997], for example, found differences of up to $\sim 25°$ in longitude between kinematically mapped crossings of the HCS at Wind (1 AU) and Ulysses (1.4 AU) and the location of the neutral line as inferred from the Stanford source surface magnetic field model. They suggested that the difference might be explained by (1) an incorrect southward displacement of the source surface model or (2) errors introduced from the simple mapping technique. *Burton et al.* [1994] analyzed a set of HCS crossings during the maximum of solar cycle 21. They found that the orientation of the HCS at 1 AU agreed well with its predicted orientation using a source surface model, suggesting that interplanetary dynamics had little effect on the orientation of the HCS, at least out to 1 AU. One of the objectives of the current study is to investigate the importance of interplanetary dynamical effects, particularly in the range 1 AU $< R <$5 AU.

[5]   *Suess and Hildner* [1985] incorporated first-order kinematics to investigate how solar wind velocity gradients might deform the HCS in the heliosphere. They found that velocity gradients of only a few kilometers per second could produce order of magnitude changes in the shape of the HCS within 20 AU. *Pizzo* [1994b] modeled the deformation of the HCS out to 30 AU using an idealized, tilted dipole three-dimensional(3-D) MHD model. He found that the inclusion of dynamic effects could lead to significant

folding of the HCS within 5 AU, and by 10 AU, shock fronts bounding CIRs had overtaken the HCS generating sharp bends in it.

[6] In this report we apply an empirically driven, 3-D, time-dependent MHD model to specific time periods during solar cycle 22 to explore the evolution of the heliospheric current sheet over the course of a solar cycle. We compare the location of the HCS as determined by the MHD model with the simpler constant-speed mapping technique to determine how important dynamical effects are. We also use the model to explore the shape of the HCS during a unique time interval of solar cycle 23 when both poles of the Sun shared the same polarity, and we compare Ulysses observations during this time with the simulation results to illustrate the value of the simulations in providing a global context for interpreting in situ observations.

2. Description of the Model

[7] We use a 3-D, time-dependent MHD model, driven by the observed line-of-sight photospheric magnetic field, to model the structure of the inner heliosphere (1 solar radii, R_S, to 5 AU). The details of the algorithm have been discussed by *Mikić et al.* [1999] and *Linker et al.* [1999] (and references therein), and its extension from the solar corona to the inner heliosphere is discussed by *Riley et al.* [2001a, 2001b]. Briefly speaking, we separate the region of space from 1 R_S to 5 AU into two distinct regions: the coronal model, which spans 1 to 30 R_S, and the heliospheric model, which spans 30 R_S to 5 AU. Such an approach is both computationally more efficient and produces a more realistic heliospheric environment. We present only results from the heliospheric solution in this report, and the coronal component may be thought of simply as a method of prescribing the inner boundary conditions of the heliospheric model.

[8] The heliospheric boundary conditions are specified in the following way. First, we directly input the radial component of the magnetic field as calculated in the coronal solution. Second, we compute the speed using the coronal magnetic configuration: At 1 R_S we set the radial speed to be some value, v_{slow}, at the boundary between open and closed field lines over a width of $\sim 6°$ (in a direction normal to the boundary) and smoothly raise it to v_{fast} over $\sim 3°$. We then map this speed profile outward along the open field lines to 30 R_S. Although this may appear somewhat ad hoc, it is based on the commonly held view that fast wind emanates from within coronal holes and slow wind is associated with the boundary between open and closed fields, as would be the case if closed field lines were sporadically opened, through magnetic reconnection. Third, we assume momentum flux balance at the inner boundary, which specifies the plasma density. Fourth, we assume thermal pressure balance, giving the temperature. Comparisons with in situ observations suggest that this approach is capable of reproducing the essential features of the large-scale structure of the inner heliosphere for a variety of solar conditions [*Riley et al.*, 2001a, 2001b].

[9] *Riley et al.* [2001a, 2001b] have discussed the approximations of this model in detail. Here we make a few brief remarks. First, we neglect the effect of pickup ions, which are thought to dominate the internal energy of

the solar wind beyond 6–10 AU [*Axford*, 1972]. Thus we limit our modeling region to $\sim$ 5 AU. Second, we neglect the effects of differential rotation, which may play a role in connecting high-latitude field lines near the Sun with lower-latitude interaction regions much further away [*Fisk*, 1996]. Third, although our MHD model is time-dependent, we assume that the flow at the inner boundary is time-stationary. Thus the flow at the inner boundary rotates rigidly with a period of 25.38 days, and spatial variations are responsible for the generation of dynamic phenomena in the solution. Consequently, our results do not include transient phenomena such as coronal mass ejections. Finally, the grid resolution necessary to model a region of space spanning 5 AU in radius precludes us from accurately modeling shock waves. However, since we would not expect shock waves to overtake, and hence alter the shape of the HCS within 8–10 AU, this limitation has no obvious impact on our results.

[10] Since the model, as implemented here, is driven by synoptic maps of the line-of-sight photospheric magnetic field observed at the Kitt Peak observatory, each solution describes an "average" picture for that Carrington rotation. In addition, while the solution does not contain any transient phenomena such as coronal mass ejecta, it can be interpreted as the "underlying" solution, assuming that the magnetic configuration responsible for the transient event returned to its initial state after eruption. As we will demonstrate, even under solar maximum conditions, such an approach can produce results that compare favorably with in situ observations. Moreover, we will show that the derived structure can persist for several or more rotations before substantial changes occur.

3. Results

[11] We begin our exploration of the large-scale structure of the HCS during the course of the solar cycle, by summarizing several solar parameters, measured over a period of 2.5 cycles, together with a selection of simulation results in Figure 1. The two central panels include data from cycles 21, 22, and the ascending phase of 23. The lower-central panel shows the monthly (yearly) averaged values of sunspot number in red (blue).

[12] The upper-central panel in Figure 1 is similar in form to the so-called butterfly diagram and summarizes the m = 0 azimuthally symmetric part of the radial component of the magnetic field, as inferred from Kitt Peak synoptic maps, for each Carrington rotation. Blue indicates inward polarity and red indicates outward polarity. These patterns describe the emergence of active regions and their associated magnetic flux at midlatitudes, their transport and diffusion, and their eventual annihilation. In addition, flux from the trailing parts of active regions can be seen to migrate steadily poleward.

[13] The HCS, as computed from the MHD model, for 11 Carrington rotations spanning solar cycle 22 and covering mid-1986 to mid-1996, are shown above and below the central panels. Time runs from the top left to right and then from the bottom left to right. Each simulation is separated from the next by $\sim$ 13 Carrington rotations. The maximum latitudinal extent of these isosurfaces is in qualitative agreement with variations in yearly smoothed sunspot number: in
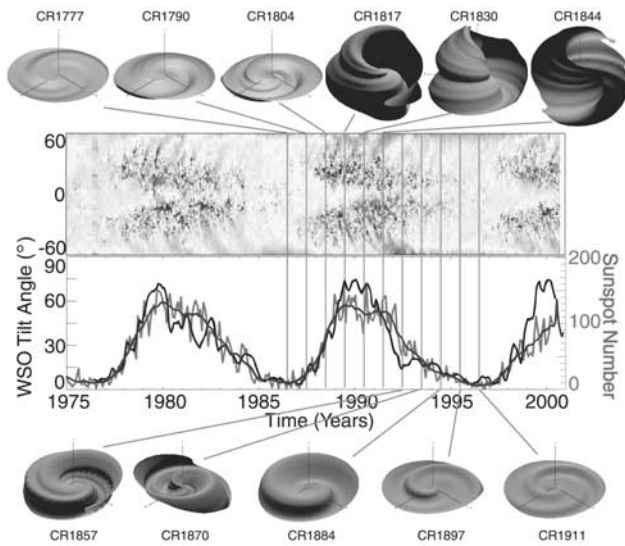
Figure 1. Evolution of several solar parameters during cycles 21, 22, and the ascending phase of 23, with emphasis on the evolution of the heliospheric current sheet (HCS) during solar cycle 22. The lower central panel shows the monthly (yearly) averaged values of sunspot number in red (blue). The upper central panel shows the $m = 0$ azimuthally symmetric part of the radial component of the magnetic field, as inferred from Kitt Peak synoptic maps, for each Carrington rotation. Blue indicates inward polarity, and red indicates outward polarity. The HCSs as computed by the MHD model (out to 5 AU) for 11 Carrington rotations, covering mid-1986 to mid-1996, are shown above and below the central panels. Time runs from the top left to right and then from the bottom left to right. WSO, Wilcox Solar observatory. See color version of this figure at back of this issue.

particular, the rapid growth of the HCS to high heliographic latitudes during the ascending phase and the slower decline during the descending phase. The profiles can be broadly grouped into three distinct categories, based on their morphology: (1) the first three rotations (CR1777, CR1790, and CR1804) during the rising portion of the solar cycle; (2) the next three rotations at solar maximum (CR1817, CR1830, and CR1844); and (3) the final five rotations during the declining phase (CR1857, CR1870, CR1884, CR1897, and CR1911). This categorization is mirrored in the yearly smoothed sunspot number, which shows a rise, a flat portion, and a longer decay. More detailed inspection of the isosurfaces reveals several noteworthy features. First, surrounding solar minimum, the HCS is better described as a flat surface with one or more folds in it, in contrast to the sinusoidal picture that is generated by considering the interplanetary extension of a tilted dipole. Alternatively, one can think of the neutral line as being warped. Second, folds in the HCS are typically asymmetric with respect to heliocentric distance: A fold rises more sharply on the inner radial side and falls more slowly on the outer radial slide. This is a natural consequence of the dynamic interaction of the surrounding streams and is particularly effective near solar minimum. Equivalently, folds are also asymmetric with respect to heliographic longitude. A northward excur-

sion of the HCS, for example, is "pulled" toward the west (larger longitudes). Adopting a simplified picture of slow solar wind flow being organized about the HCS, and faster flow elsewhere, this asymmetry can be understood by the "stretching" of the HCS on the outer portion of the fold, where a rarefaction region is developing and slower flow is being accelerated into it. Meanwhile, on the inner side the HCS fold is being steepened owing to the formation of a compression region. Fourth, near solar maximum the HCS is often vertical over large ranges in latitude.

[14] Spatial variability at the Sun dominates the large-scale dynamical structure of the heliosphere during the declining phase and solar minimum, leading to time-stationary structure in the corotating frame of reference. In contrast, temporal variations, and coronal mass ejections in particular, undoubtedly play a more important role at solar maximum. Our simulations, however, suggest that while time-dependent phenomena may be important, the underlying pattern from one rotation to the next is often well maintained. To illustrate this, we display the HCS for Carrington rotations 1945 through 1948 in Figure 2. Note that the overall features of the HCS (maximum extent, phase, etc.) are relatively stable from one rotation to the next. In reality, this picture would be more complicated and probably disrupted by the passage of coronal mass ejections (CMEs).

[15] The latitude of the MHD-computed HCS at three heliocentric distances is shown in Figure 3 (black curve) for Carrington rotation 1913. We have previously shown that the model agrees well with Wind measurements taken during this time period [*Linker et al.*, 1999]. From top to bottom the panels show traces at 30 R_S, 2.5 AU, and 5 AU. Also shown are traces of the latitude of the HCS, calculated assuming a constant speed mapping of the trace from 30 R_S. The two speeds correspond to the average (blue) and
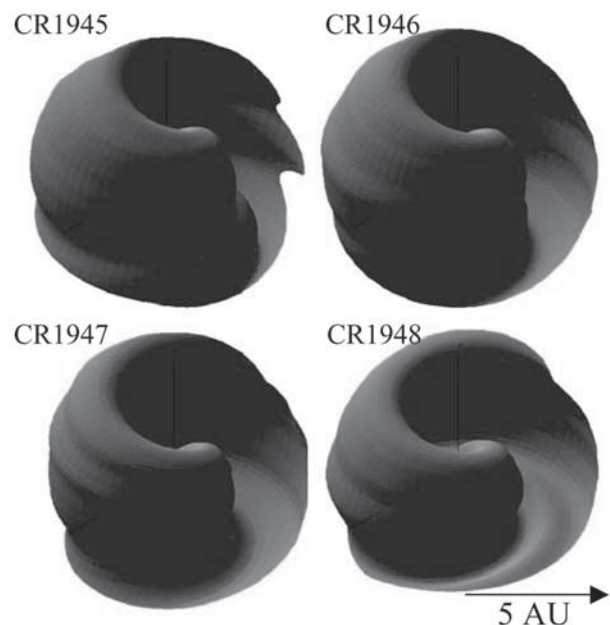

Figure 2. The HCS during four consecutive Carrington rotations, 1945–1948, covering the time period of 12 January 1999 to 1 May 1999.
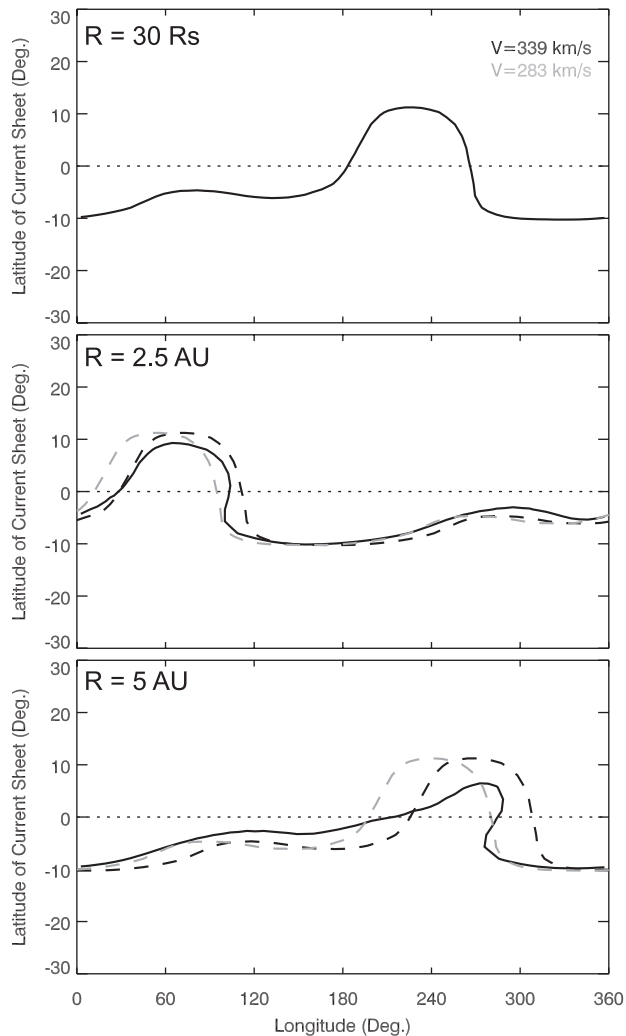
Figure 3. Latitude of the HCS at three heliocentric distances: (top) 30 R_S, (middle) 2.5 AU, and (bottom) 5 AU for Carrington rotation 1913 (22 August to 18 September 1996). The MHD result is shown as the solid black curve. The two dashed curves are based on a ballistic mapping of the MHD-derived HCS at $30R_S$, using the average (black) and the median (gray) solar wind speed at that distance.

median (green) that were present in the simulation at the location of the HCS. The constant speed mappings differ only in their longitudinal phase, being related by the fact that longitudes, distances, and speeds are interchangeable through the relationship $\phi = \omega_{rot} r/v$, where v is the speed of the parcel of plasma, r is the heliocentric distance over which the parcel has traveled, and ω_{rot} is the rotation rate. From these comparisons it is apparent that an accurate estimate for the speed of the plasma surrounding the HCS is necessary if the constant-speed mapping technique is going to be employed. More importantly, however, by 2.5 AU the MHD solution and the constant-speed mapping differ qualitatively. The fold in the MHD solution has "steepened" to the extent that its westward (right) side is double-valued. By 5 AU this steepening dominates the profile of the fold, and the constant-speed mappings cannot

replicate the profile produced by the MHD solution. Another effect that is not present in the simpler technique is a decease in maximum latitudinal extent with increasing distance from the Sun. This behavior is a consequence of magnetic pressure gradients at the inner boundary of the heliospheric model and a point that we will return to later.

[16] At solar maximum, although the Sun and heliosphere are significantly more complex in appearance, surprisingly, the evolution of the HCS is simpler. To illustrate this, in Figure 4 we summarize the latitude of the HCS during Carrington rotation 1961 from the late ascending phase of cycle 23. Comparing the MHD solution (black curve) at the three heliocentric distances shows that while smaller-scale irregularities are generated, the profile remains relatively unchanged. Moreover, the constant-speed mapping of the HCS (at the appropriate speed of 330 km s^{-1}) provides a reasonable approximation to the MHD solution. This result is due to the lack of appreciable interaction regions during solar maximum; substantial differences in speed and density are required to compress and rarefy plasma, causing it to accelerate and decelerate. At solar maximum, however, high-speed flows are limited to isolated holes. They do not have the same driving force in the solar wind, and as these
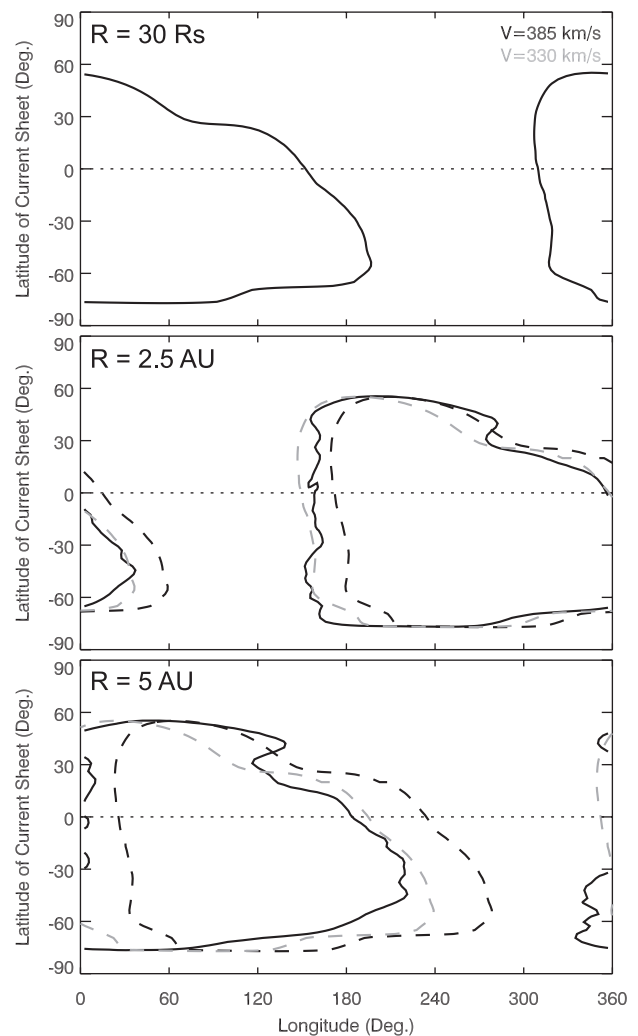

Figure 4. Same as Figure 3 but for Carrington rotation 1961 (23 March to 19 April 2000).
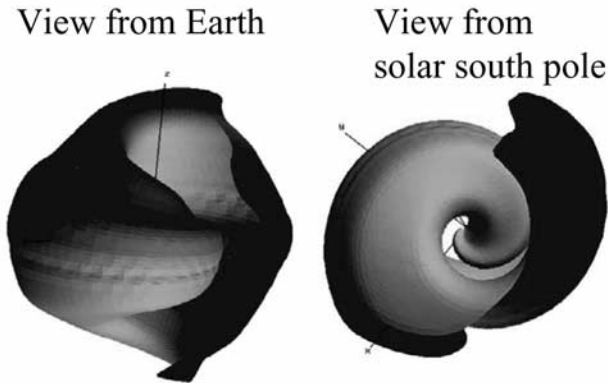
Figure 5. Two views of the heliospheric current sheet (out to 5 AU): (left) the view from Earth and (right) the view from above the south pole of the Sun.

"beams" propagate outward into the solar wind, they become attenuated. The net result is that the HCS is not pulled and pushed around as much as it is during the declining phase of the solar cycle and solar minimum.

[17] The global shape of the HCS computed for CR1961 is shown in Figure 5. The two views show how the HCS would look from Earth (Figure 5, left) and the south pole of the Sun (Figure 5, right). The HCS separates inwardly and outwardly directed magnetic field lines. Typically, it also separates the two poles of the Sun. During the time surrounding Carrington rotation 1961, however, both poles of the Sun were of the same magnetic polarity, leading to the unique topology of the HCS illustrated in Figure 5. This can be seen in the synoptic photospheric maps produced by the Kitt Peak observatory ftp://ftp.noao.edu/kpvt/synoptic/mag). Given such an input, the combination of solar rotation and the supersonic radial flow of the solar wind away from the Sun generates the "conch shell"-like isosurface shown.

[18] The strength of these simulations in providing the global context for interpreting in situ observations is illustrated in Figure 6, where we compare Ulysses observations of the polarity of the interplanetary magnetic field (IMF) [Balogh et al., 1992] with the MHD model derived for CR1961. Ulysses had passed from the Northern Hemisphere into the Southern Hemisphere at aphelion and was moving toward the south pole of the Sun for a second time. The observations run from right to left with increasing time. On their own these measurements are suggestive of a dipole-like field, as would have been seen during the late declining phase and minimum of the solar activity cycle. Only when the model-derived HCS is overlaid can we appreciate the global context of the Ulysses observations. Although the sector crossings (i.e., the reversals in polarity) do not match exactly, their qualitative alignment suggests that the model is, at least on the large scale, a relatively good picture of the inner heliosphere.

4. Summary and Conclusions

[19] In this report we have, for the first time, used 3-D MHD simulations to model the large-scale structure of the HCS during the course of a solar cycle. By comparison with the simpler "ballistic" mapping technique for generating the shape of the HCS in the solar wind, we have shown that

dynamic effects can play an important role in changing the morphology of the HCS. We have also used the model to explore the unusual "conch shell" shape of the HCS during Carrington rotation 1961, which occurred toward the maximum of solar cycle 23. Comparison with Ulysses observations illustrates one of the strengths of the model in being able to provide a global perspective with which to interpret in situ observations.

[20] Our results indicate that, particularly near solar minimum, interplanetary dynamics can distort the HCS significantly. Even during CR1913, when the neutral line was essentially flat except for a localized northward excursion near ~250° longitude [Riley et al., 1999], by several AU the HCS had become double-valued in longitude. We note that it is also possible for the neutral line to double back in longitude back at the Sun. In fact, Shodhan et al. [1994] found that over a solar cycle the neutral line doubles back on itself in longitude about one third of the time. The effect of interplanetary dynamics for such configurations would be to accentuate the corrugations further. These results are not inconsistent with the study by Burton et al. [1994], which suggested that interplanetary dynamics were not a significant effect between the Sun and 1 AU. Dynamical effects are cumulative, and while ballistic mapping might represent an acceptable approximation within 1 AU, it becomes progressively worse at larger distances. Our results suggest that beyond ~2 AU, dynamic effects must be included.

[21] It is worth noting that above ~75°, constraints imposed from viewing the Sun from the Earth make photospheric measurements difficult. In particular, determining the polar field strengths can have a significant effect on determining the latitudinal extent of the HCS [Hoeksema et al., 1982]. This is especially true at solar minimum when the polar fields are strongest. On the other hand, the loss of large polar coronal holes near solar maximum, being replaced by more complex field configurations, makes modeling the polar regions themselves a more challenging task [e.g., Mikić et al., 1999].
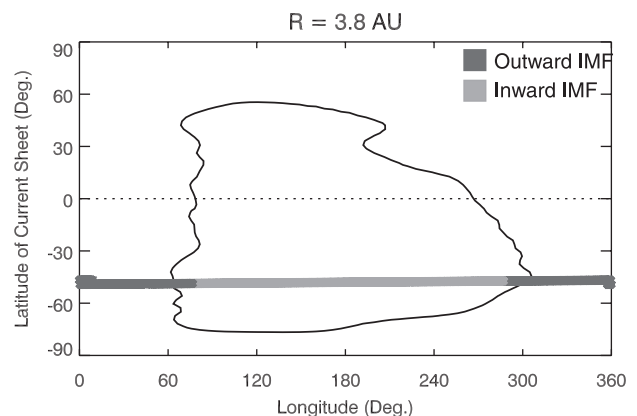

Figure 6. Latitude of the HCS at 3.8 AU, coinciding with the heliocentric position of the Ulysses spacecraft at this time (Carrington rotation 1961). The Ulysses trajectory is shown as the thick dark gray/light gray curve and progresses from right to left with increasing time. Dark gray indicates measured outward interplanetary magnetic field (IMF), and light gray indicates inward IMF.

[22] In addition to longitudinal distortions, some of our simulations suggest that the HCS can evolve in latitude. Figure 3, for example, implies that by 5 AU the maximum extent of the HCS in the Northern Hemisphere decreased by $\sim4°$ from its value at the Sun. This evolution is directly related to the specification of our boundary conditions and so must be viewed with caution. At the inner boundary of the heliospheric model, we chose to impose thermal pressure balance rather than total pressure balance. Thus pressure gradients corresponding to variations in the radial component of the magnetic field generate meridional flows responsible for the latitudinal change in the maximum extent of the HCS. In reality, by 30 R_S, we would expect transverse pressure forces to have already equilibrated meridional flows to have already been generated. Our numerical "game" generates these flows at 30 R_S. Although we cannot reliably prescribe such gradients for any specific interval of time, this exercise allows us to infer that if present, we could expect deviations of $\sim5°$ in latitude over 5 AU. Often, we see no appreciable change in latitude with increasing distance from the Sun. This flattening is most prevalent near solar minimum when the polar fields tend to be stronger, driving pressure gradients that result in equatorward motion of plasma and hence a flattening in the maximum extent of the HCS.

[23] We reiterate that the solutions described here represent, in a sense, an average over a solar rotation. We assumed that the photospheric magnetic field measured around central meridian did not change substantially during a solar rotation, and so it is likely that the shape of the HCS would be quantitatively different at longitudes progressively further away from the Earth-Sun line. Nevertheless, we found that even under solar maximum conditions, the shape of the HCS remains qualitatively the same for several solar rotations. Thus, even under more active times, this approach appears to be valid. More importantly, however, we have not addressed how CMEs or other transient phenomena might affect these results. Within the framework of the current model this is a challenging task that we intend to pursue in the future. Instead, we should view the HCS as calculated here as an "equilibrium" picture and bear in mind that the HCS may be significantly distorted by the passage of fast CMEs.

References

Akasofu, S. I., and C. D. Fry, Heliospheric current sheet and its solar cycle variations, *J. Geophys. Res.*, *91*, 13,679, 1986.

Axford, W. I., Interaction of the solar wind with the interstellar medium, in *Solar Wind*, edited by C. P. Sonett, P. J. Coleman, and J. M. Wilcox, NASA Spec. Publ., *NASA SP-308*, 609, 1972.

Balogh, A., T. J. Beek, R. J. Forsyth, P. C. Hedgecock, R. J. Marquedant, E. J. Smith, D. J. Southward, and B. T. Tsurutani, The magnetic field investigation on the Ulysses mission: Instrumentation and preliminary scientific results, *Astron. Astrophys*, *92*, 221, 1992.

Burton, M. E., N. U. Crooker, G. L. Siscoe, and E. J. Smith, A test of source-surface model predictions of heliospheric current sheet inclination, *J. Geophys. Res.*, *99*, 1, 1994.

Fisk, L. A., Motion of the footpoints of heliospheric magnetic field lines at the Sun: Implications for recurrent energetic particle events at high heliographic latitudes, *J. Geophys. Res.*, *101*, 15,547, 1996.

Ho, C. M., B. T. Tsurutani, J. K. Arballo, B. E. Goldstein, R. L. Lepping, K. W. Ogilvie, A. J. Lazarus, and J. T. Steinberg, Latitudinal structure of the heliospheric current sheet and corotating streams measured by Wind and Ulysses, *Geophys. Res. Lett.*, *24*, 915, 1997.

Hoeksema, J. T., J. M. Wilcox, and P. H. Scherrer, Structure of the heliospheric current sheet in the early portion of sunspot cycle 21, *J. Geophys. Res.*, *87*, 10,331, 1982.

Jokipii, R. J., Transport and acceleration of energetic particles in winds, in *Cosmic Winds and the Heliosphere*, edited by J. R. Jokipii, C. P. Sonett, and M. S. Giampapa, p. 833, Univ. of Ariz. Press, Tucson, 1997.

Linker, J. A., Z. Mikić, D. A. Bisecker, R. J. Forsyth, S. E. Gibson, A. J. Lazarus, A. Lecinski, P. Riley, A. Szabo, and B. J. Thompson, Magnetohydrodynamic modeling of the solar corona during whole Sun month, *J. Geophys. Res.*, *104*, 9809, 1999.

Mikić, Z., J. A. Linker, D. D. Schnack, R. Lionello, and A. Tarditi, Magnetohydrodynamic modeling of the global solar corona, *Phys. Plasmas*, *6*, 2217, 1999.

Pizzo, V. J., Global, quasi-steady dynamics of the distant solar wind, 1, Origin of north-south flows in the outer heliosphere, *J. Geophys. Res.*, *99*, 4173, 1994a.

Pizzo, V. J., Global, quasi-steady dynamics of the distant solar wind, 2, Deformation of the heliospheric current sheet, *J. Geophys. Res.*, *99*, 4185, 1994b.

Riley, P., J. T. Gosling, D. J. McComas, V. J. Pizzo, J. G. Luhmann, D. Biesecker, R. J. Forsyth, J. T. Hoeksema, A. Lecinski, and B. J. Thompson, Relationship between Ulysses plasma observations and solar observations during the whole Sun month campaign, *J. Geophys. Res.*, *104*, 9871, 1999.

Riley, P., J. A. Linker, and Z. Mikić, An empirically-driven global MHD model of the corona and inner heliosphere, *J. Geophys. Res.*, *106*, 15,889, 2001a.

Riley, P., J. A. Linker, Z. Mikić, and R. Lionello, MHD modeling of the solar corona and inner heliosphere: Comparison with observations, in *Space Weather, Geophys. Monogr. Ser.*, vol. 125, edited by P. Song, H. J. Singer, and G. L. Siscoe, p. 159, AGU, Washington, D.C., 2001b.

Sanderson, T. R., D. Lario, M. Maksimovic, R. G. Marsden, C. Tranquille, A. Balogh, R. J. Forsyth, and B. E. Goldstein, Current sheet control of recurrent particle increase at 4–5 AU, *Geophys. Res. Lett.*, *26*, 1785, 1999.

Shodhan, S., N. U. Crooker, W. J. Hughes, and G. L. Siscoe, Heliospheric current sheet inclinations predicted from source surface maps, *J. Geophys. Res.*, *99*, 2531, 1994.

Suess, S. T., and E. Hildner, Deformation of the heliospheric current sheet, *J. Geophys. Res.*, *90*, 9461, 1985.

J. A. Linker, Z. Mikić, and P. Riley, Science Applications International Corporation, San Diego, CA 92121, USA. (linker@iris023.saic.com; mikic@iris023.saic.com; pete.riley@saic.com)
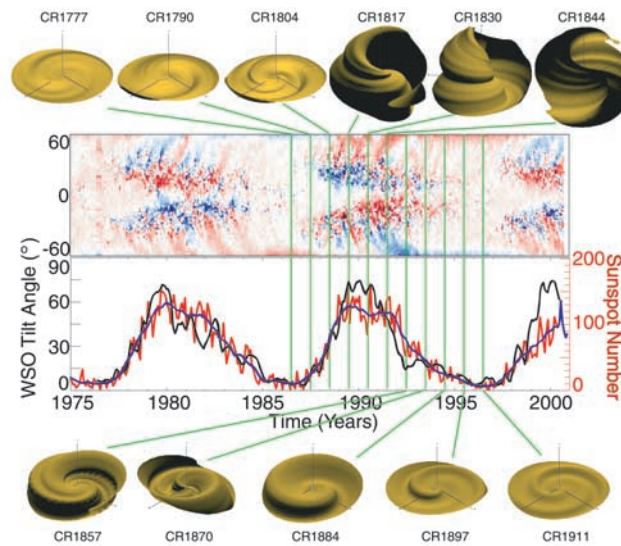
Figure 1. Evolution of several solar parameters during cycles 21, 22, and the ascending phase of 23, with emphasis on the evolution of the heliospheric current sheet (HCS) during solar cycle 22. The lower central panel shows the monthly (yearly) averaged values of sunspot number in red (blue). The upper central panel shows the $m = 0$ azimuthally symmetric part of the radial component of the magnetic field, as inferred from Kitt Peak synoptic maps, for each Carrington rotation. Blue indicates inward polarity, and red indicates outward polarity. The HCSs as computed by the MHD model (out to 5 AU) for 11 Carrington rotations, covering mid-1986 to mid-1996, are shown above and below the central panels. Time runs from the top left to right and then from the bottom left to right. WSO, Wilcox Solar observatory.